Anal. Bioanal. Electrochem., Vol. 10, No. 1, 2018, 1-17

Analytical & Bioanalytical Electrochemistry

2018 by CEE
www.abechem.com

Full Paper

Lithium Cobalt Oxide as Lithium Ion Battery Cathode Materials Prepared by Flame Spray Pyrolysis Method

Hadi Mohammadi,[1] Mohsen Khosravi[2] and Seyed Mohammad Jafari[3,*]

[1]*Master graduate of Nanomaterials, Department of Nanotechnology Engineering, University of Isfahan, Isfahan, I. R. Iran*
[2]*Department of Nanotechnology Engineering, Faculty of Advanced Science and Technologies, University of Isfahan, Isfahan, 81744-73441, Iran*
[3]*PhD student of Nanophysics, Tendency of Nanostructures, Faculty of Science, University of Zanjan, Zanjan, I. R. Iran*

*Corresponding Author, Tel.: +98 9132 221711; Fax: 98139-47395
E-Mail: s.m.jafari@znu.ac.ir, mohammadjaffari.1711@yahoo.com

Received: 3 May 2017 / Received in revised form: 28 June 2017 /
Accepted: 20 November 2017 / Published online: 31 January 2018

Abstract- Lithium ion batteries are considered the most promising energy storage and conversion device candidates for use in future electric vehicle applications due to their ultrahigh energy density. In this study, a facile, ultrafast and green flame spray pyrolysis method was developed well to efficiently fabricate submicron-sized lithium cobaltite spheres from an aqueous spray solution of lithium nitrate and cobalt nitrate. Molar ratios of lithium: cobalt in the precursor solution was altered at three different levels, viz., 1: 1, 1.3: 1 and 1.7: 1. Then samples obtained under same conditions were calcined. Also, sample obtained with molar ratios of lithium: cobalt 1.7: 1, under different conditions atmosphere was calcined. The sample calcined in oxygen atmosphere with low flow was phase pure crystalline rhombohedral lithium cobalt oxide. Furthermore, this sample showed an acceptable performance as cathode active material of lithium ion battery. The rechargeable capacity was 162 mAh g^{-1} at 0.1 C and 101 mAh g^{-1} at 1 C and capacity retention of 84% after 50 cycles at this rate for this sample was observed.

Keywords- Lithium ion batteries, Flame spray pyrolysis, Cathode active material, Lithium cobalt oxide, Layer structure

1. INTRODUCTION

Energy production and consumption that rely on the combustion of fossil fuels have had severe impacts on world economics and ecology [1]. Electrochemical energy conversion and storage systems, which include batteries, fuel cells, and supercapacitors, are undoubtedly playing a very important role as an alternative because the energy consumption is designed to be more sustainable and more environmentally friendly [2]. The lithium-ion battery is now the prevailing rechargeable battery; it is used in many portable electronic devices such as cell phones and notebook computers, because of the long cycling life and of an energy density higher than that of other rechargeable batteries [3-5]. The layered structure lithium cobalt oxide (LCO) is one of the earliest founded lithium metal oxides used as cathode materials [6,7]. Good performance and stability make it the main commercially used cathode material for more than a quarter of a century, despite toxicity and high cost [8]. It has been the subject of literally 1000s of papers [9]. The improvements in capacity and recharge ability still require development of a new process to synthesize LCO particles with suitable characteristics.

Many methods have been employed for synthesis of LCO cathode such as solid-state, sol-gel, co-precipitation, combustion, spray pyrolysis, microwave and hydrothermal methods [10-16]. Even though many of these methods have proved to be useful at laboratory-scale synthesis, the complexity and cost implications of scaling such methods to industrial manufacturing often proved to be unfeasible [14]. Over the years one method, spray pyrolysis, proved to be successful at both laboratory-scale and industrial level. The spray pyrolysis method shows versatility in its approach to incorporate a variety of chemical compositions and techniques that can be scaled to industrial feasible processes with relative ease [9,14,17,18].

Flame aerosol technology, especially flame-spray pyrolysis (FSP) is thought to be an effective technique for the creation of new and sophisticated materials for catalysis, sensors, photoluminescence, biomaterials and batteries [19-29]. This method was invented by the Laine group in the early 1990's [30]. Produced powders are lightly agglomerated but not aggregated due to rapid quenching. Other advantages are process efficiency, product quality and easy control of compositions, which is done by simply modifying the precursor solution [9,31,32].

To better control the nanoparticle properties such as particle size, size distribution, and morphology requires an understanding of the effects of main factors during the FSP [33]. Main factors affecting the particle properties include precursor concentration, droplet size, gas flow rates, and flame characteristics [23,33-35].

Herein, we report Liquid-feed flame spray pyrolysis (LF-FSP) synthesis of Submicron-sized LCO as LIB cathode active material with nitrate salts of lithium and cobalt as precursors. The influence of molar ratios of lithium: cobalt in the precursor solution and

calcination environment on the structure and electrochemical performance of the LCO powders will be presented and discussed. The results suggest that FSP holds potential for rapid production of cathode materials with low-cost nitrate precursors and minimal energy input.

2. EXPERIMENTAL SECTION

2.1. Synthesis of lithium cobalt oxide powders

Submicron-sized LCO powders were synthesized with flame spray pyrolysis (FSP) method and subsequent heat treatment. The details of FSP apparatus used in this study are described in the following.

A schematic of the used apparatus for the preparation of LCO particles is shown in Fig. 1. This apparatus is consists of an ultrasonic atomizer for aerosol precursor, a turbulent flame, cooling system, particles collector system and pump.

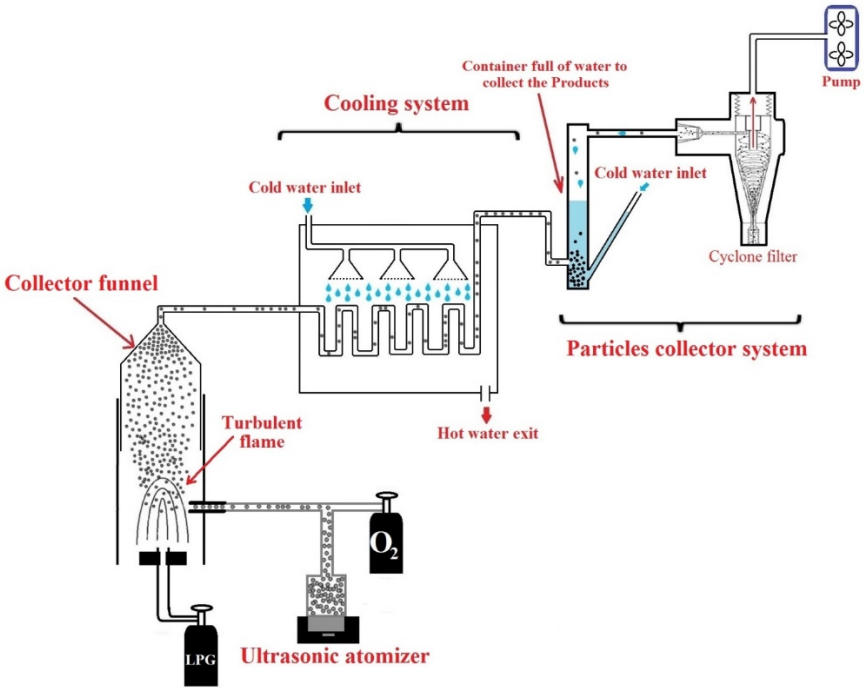

Fig. 1. A schematic of the used apparatus for the synthesis of particles

The solution prepared (described in the next section) was aerosolized with an ultrasonic nebulizer (at a frequency of about 1 MHz). The atomized droplets were carried by nitrogen carrier gas into a flame hydrolysis reaction zone in an oxy-hydrogen torch. Liquefied petroleum gas (LPG) and oxygen were used as the fuel and oxidizer, respectively, in order to create a turbulent flame. The flow rates of the fuel, oxidizer, and carrier gases were maintained at 5, 40 and 10 L min^{-1}, respectively. The cooling system consists of an aluminum container, aluminum pipes, water pumps, showers and water entry and exit valves. In this

system, water via domestic shower was poured on aluminum pipes, which this will be cooling the products before collecting.

After the cooling stage a large percentage of products was initially was collected in a tube of filled with water. The product inlet pipe is placed at the bottom of the tube of filled with water; this caused turbulence in the water and ultimately collects the product. The pump inlet is at the top of the tube where this is far from the water surface; this distance will prevent from being attracted water into the pump. Cyclone filter is also employed as collector assistance and to ensure full collection products. This filter is used before the entrance pump. Finally to separate the synthesized particles are collected water in the container filled with water and water in cyclone filter. Particles were obtained after centrifugation.

2.2. Synthesis of lithium cobalt oxide powders

For the aerosol flame synthesis process, an aqueous precursor solution was prepared by dissolving Co $(No_3)_2 \cdot 6H_2O$ (Dae Jung, above 97%) and $LiNO_3$ (Dae Jung, above 97%) in deionized water at a concentration of 0.2 mol L^{-1} and with Co: Li molar ratio 1: 1 and it was nebulized with a domestic ultrasonic nebulizer (35 watts). After collection and centrifugation the obtained particles by the apparatus were described in the previous section (Fig. 1), the sample because to be completely dry was placed in a vacuum oven at 150 °C for 2 h, which is designated as LCO-A.

A series of samples by altering of the amount of Co: Li molar ratio including 1.3: 1 and 1.7: 1 (Table 1) were also prepared for comparison. The final products were called LCO-B and LCO-C, respectively.

Table 1. Composition of Co $(No_3)_2 \cdot 6H_2O$ and $LiNo_3$ and codes of the corresponding LCOs

LCO code	Concentration (mol L^{-1})	Molar ratio (Co:Li)
LCO-A	0.2	1.0:1
LCO-B	0.2	1.3:1
LCO-C	0.2	1.7:1

Subsequently, the as-synthesized powder was heat-treated at 5 °C/ minute up to 800 °C and soaking for 2 h in tube furnace (TF5/25-1500) under air atmosphere, in order to remove impure phases and improve crystallinity, which is designated as LCO-A-1, LCO-B-1 and LCO-C-1.

Also, to examine the effect of calcination environment, the powder of LCO-C (Table 1) was chosen and calcinated with four further different environment; air with slow rate (5 L min^{-1}), air with fast rate (20 L min^{-1}), oxygen with slow rate and oxygen with fast rate, whose

derived LCOs are herein after denoted as LCO-C-2, LCO-C-3, LCO-C-4 and LCO-C-5, respectively.

2.3. Physical characterization

X-ray diffraction (XRD) experiments of the LCOs were carried out from 5° to 80° 2θ with a step size of 0.05° 2θ using a D8 Advance X-ray Diffractometer (BRUKER, Germany) equipped with Co Kα radiation (λ=1.789 nm). FT-IR spectra were recorded on a JASCO 6300 spectrometer over the wavenumber range of 400–4000 cm^{-1}.

The LCO particle size and morphology were determined by using a scanning electron microscope (VEGA\\TESCAN-XMU), and diameters were measured by using Microstructural Image Processing software (MIP 4.1 full; Nahamin Pardazan Asia, I.R. Iran). Two types of mean particle sizes were calculated: number–average (D_n) and weight–average (D_w), ($D_n=\sum D_i/N$, $D_w=\sum D_i^4/\sum D_i^3$), where N is the number of particles [36]. Particle size distributions were characterized by polydispersity indices (PDI) calculated as a ratio of weight–average to number– average particle diameter.

Nitrogen adsorption–desorption measurements (Japan, BELSORP-Mini II) were carried out at liquid nitrogen temperature (77 K). Before sorption measurement, the samples were degassed for 48 h under vacuum at 250 °C. The BET surface area (S_{BET}), pore size distributions and mesopore volume (V_{me}), were determined by Brunauer–Emmett–Teller (BET) theory, Barrett–Joyner– Halenda (BJH) method, and t-plot theory, respectively.

2.4. Electrochemical measurements

The electrodes were prepared by dispersing the as-prepared LCO powders (80 wt %), carbon black (10 wt %), and poly Vinylidene fluoride binder (PVDF, 10 wt %) in N-methyl-2-pyrrolidone (NMP) to form a slurry. The mixture was simultaneously stirred and degassed under vacuum for 40 minutes. The thickness of the coated film was about 140 µm onto a 10 µm thick Aluminum foil current collector using a micrometer adjustable film applicator (Sheen instrument Co., Ltd. Shanghai, China). The as-prepared electrode was dried at 120 °C for about 20 min in a vacuum oven (Memmert, VO400 model) in air atmosphere, roll-pressed several times to enhance inter-particle contact, adjust the film thickness and help to better adhesion to the current collector. A typical final thickness of electrode after dried and roll-pressed with Aluminum foil was 60 µm. The electrode was then punched in the form of disks with a diameter of 10 mm, and dried at 120 °C for 12 h under vacuum.

The charge-discharge experiments were carried out on 128 battery tester (Kimia Pardaz Samaneh Co, I.R.Iran) with dedicated software (Kimiastat Analyzer software, Version 7.0.5) and the cyclic voltammetry (CV) were carried out using an Autolab 302N potentio-galvanostat (Metrohm Autolab B.V., the Netherlands) controlled by Nova 1.9 software. A

homemade two electrode electrochemical cell (similar to Swagelok-type cells) was used throughout. Pure Li foil was used both as counter and reference electrode. All cells were assembled in a glove box filled with high purity dry argon at room temperature. A porous polyolefin memberane was used as a separator. The electrolyte solution was 1 M $LiPF_6$ dissolved in a mixture of ethylene carbonate (EC) and dimethyl carbonate (DEC) with a volume ratio of 1: 1.

The charge-discharge measurements were performed at ambient temperature at rate of 0.1 C (1 C=280 mA g^{-1}) in the voltage range from 2.5 to 4.4 V. Cyclic voltammetry (CV) were carried out from 2.5 to 4.5 V with a scan rate of 1 mV s^{-1} in a two-electrode system. Cycling performance were carried out at 1 C between 2.5- 4.4 V for 50 cycles. Rate capability of the LCO electrodes was assessed as follows: after charge cycle at 0.1 C to 2.5 V, were discharged to 4.4 V with different current rates from 0.1 C to 7 C. All of the specific capacities mentioned in this work were estimated by using the weight of the active materials and all potential values in this paper are versus Li/Li^+ electrode.

3. RESULTS AND DISCUSION

3.1. Structural characterization

Fig. 2 shows SEM images of LCO-A and LCO-C. As can be readily seen, the powders have spherical shape. The as-synthesized particles were submicron in size, with some particles falling into the nano-size range; the average particle size of LCO-A and LCO-C is 430 nm and 480 nm with polydispersity index (PDI) of 2.7 and 2.8, respectively.

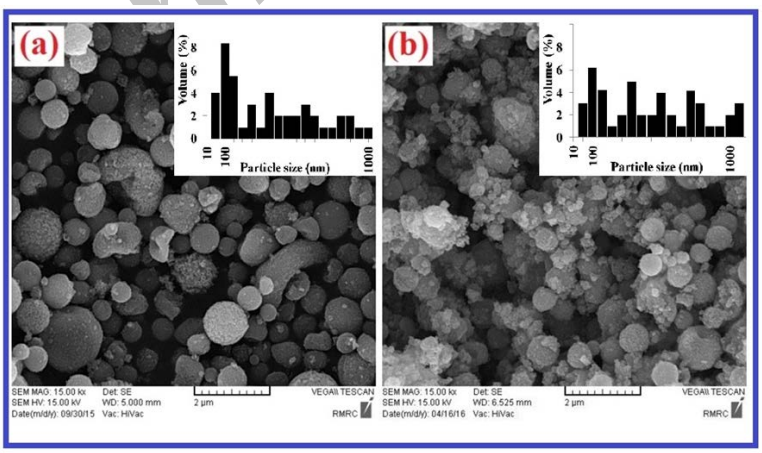

Fig. 2. SEM images of (a) LCO-A and (b) LCO-C, and insets are the corresponding statistic histogram

The corresponding statistic histograms presented in the insets of Fig. 2 show that particle size distributions of the LCOs are not uniform. The particle sizes of LCO-C is larger than

LCO-A, due to the higher molar ratio of LCO-C. By increasing the molar ratio, the frequency of collisions between particles increases; and so at the growth mechanism particle size becomes large. It also can be said, if the molar ratio of the sample is high, due to increased supersaturation, many primary buds are formed, which are stick together due to collisions in the flame, and to create larger particles. Also this non-uniform collision causes non-uniform distribution of particles.

The phase purity and crystal structure of the as-synthesized powders were investigated by XRD. Gummow et al. [37] applied Rietveld structural refinement for X-ray diffraction patterns for LCO powders.

The XRD pattern of the as-synthesized powder matched the LCO layer (rhombohedral crystal structure with space group R-3m) and Co_3O_4 cubic phase, as seen in Fig. 3(a). The wide XRD peaks of the as-synthesized powders suggest nanocrystalline structures. However, some impurities coexist with the as-synthesized powders, as indicated by the minor peaks in the XRD. The impurity was identified as Co_3O_4, which is known to form at elevated temperatures [38]. Studies have shown that at elevated temperatures, oxygen may be extracted from layer LCO, forming oxygen deficient layer [38,39]. In this study, the residence time of the particles in the flame at the high temperature region was very short, so only a small portion of layer $LiCoO_2$ decomposed into Co_3O_4. Nonetheless, a post-annealing treatment was necessary to remove the impurity in the flame-synthesized layer $LiCoO_2$.

After annealing the as-synthesized powder at 800 ˚C for 2h in air atmosphere, the XRD pattern was a good match to the single-phase layer $LiCoO_2$ with a space group R-3m, as shown in Fig. 3(b). The crystallinity of the powder was also greatly improved, as indicated by the sharper XRD peaks. Fig. 3(c) shows the XRD patterns of LCO powders calcinated at 800 ˚C for 2h in different environment.

Nanocrystallite grain sizes were determined from the FWHM of diffraction lines observed in 2θ range of 5-80°2θ on sinθ, according to Williamson-Hall's equation [40]:

$$\beta\cos\theta = k\lambda/L + 2\varepsilon \sin\theta \quad (1)$$

Where β is FWHM observed, the shape factor k was assumed to be 0.9 similar to Scherrer equation's. λ=1.789 nm (wavelength of k_α (co)). The plots of βcosθ *vs* sinθ for different samples were approximated to be linear. Lattice strain and grain size was determined from the slop and intercept of this linear relation, respectively. Because of highly-crystallized powder samples, the linearity between βcosθ and sinθ is evident [41].

The results of XRD peak analyses are summarized in Table 2. As can be seen in Table 2, grain sizes increase from 7.39 nm (for LCO-A) to 9.42 nm (for LCO-C).

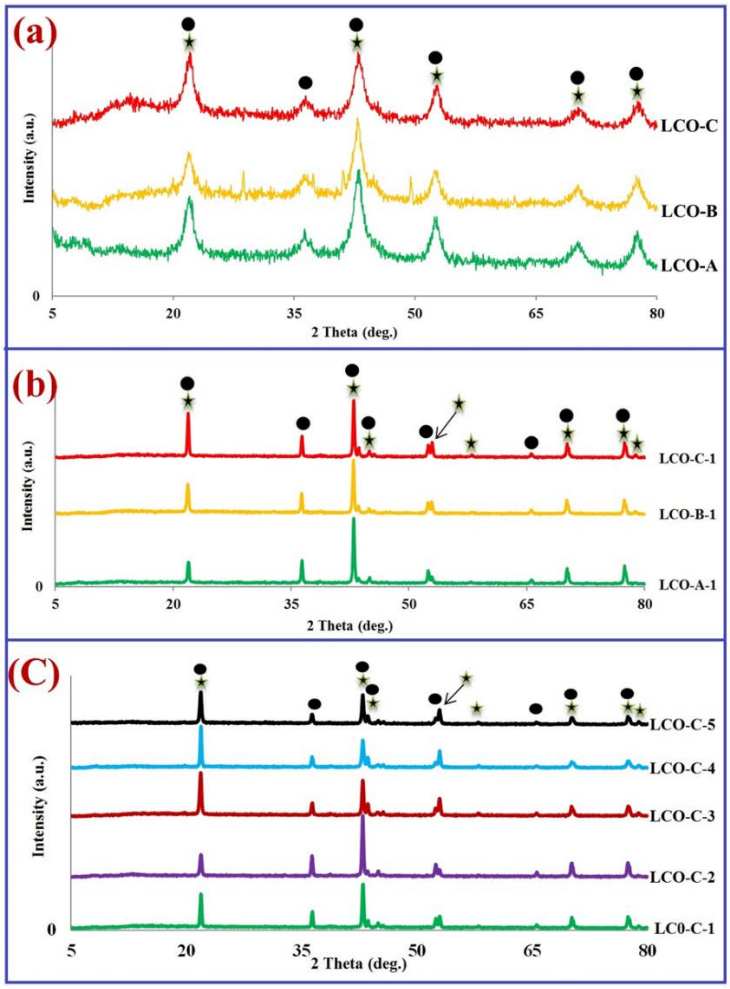

Fig. 3. X-ray diffraction patterns of LCO powders (a) before calcination (b) after calcination in air atmosphere and (c) after calcination in different environment. (Stars are peaks corresponding to LCO phases and spheres are peaks corresponding to Co_3O_4 phases.)

Table 2. XRD data extracted from Fig. 3

Sample	2θ (003)	Lattice strain	Grain size (nm)
LCO-A	22.03	0.0032	7.4
LCO-B	21.99	0.0028	9.3
LCO-C	22.18	0.0117	9.4
LCO-A-1	21.94	0.0005	36.6
LCO-B-1	21.88	0.0002	32.2
LCO-C-1	21.90	0.0016	46.0
LCO-C-2	21.91	0.0004	34.3
LCO-C-3	21.87	0.0016	37.4
LCO-C-4	21.90	0.0052	89.4
LCO-C-5	21.85	0.0017	36.6

The relationship between the amount of the different structures and electrochemical performance of LCO powders as cathode for lithium ion batteries will be discussed in the next section.

In order to investigate the presence of possible functional groups, FT-IR spectra of LCO-C-2 and LCO-C-4 are presented Fig. 4. Apart from differences in intensities, the main peaks are the same for the two samples. The peaks between 400 and 600 cm^{-1} arise from binding of Co^{3+} ions to the oxygen ions [42,43].

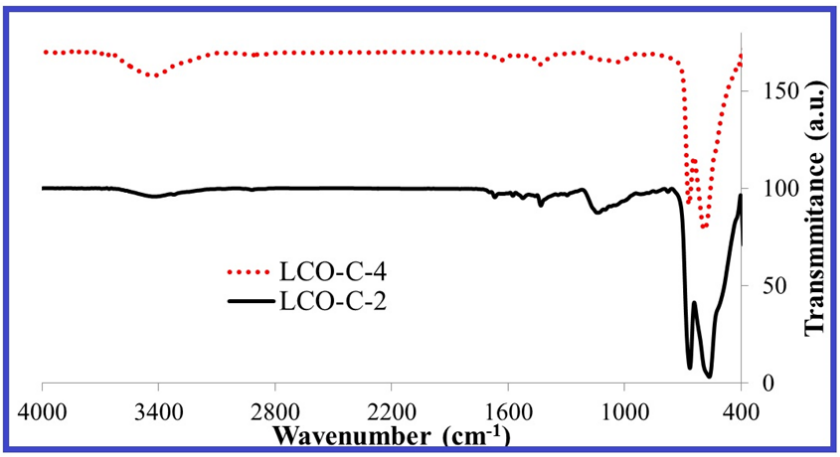

Fig. 4. FT-IR spectra of LCO-C-2 and LCO-C-4

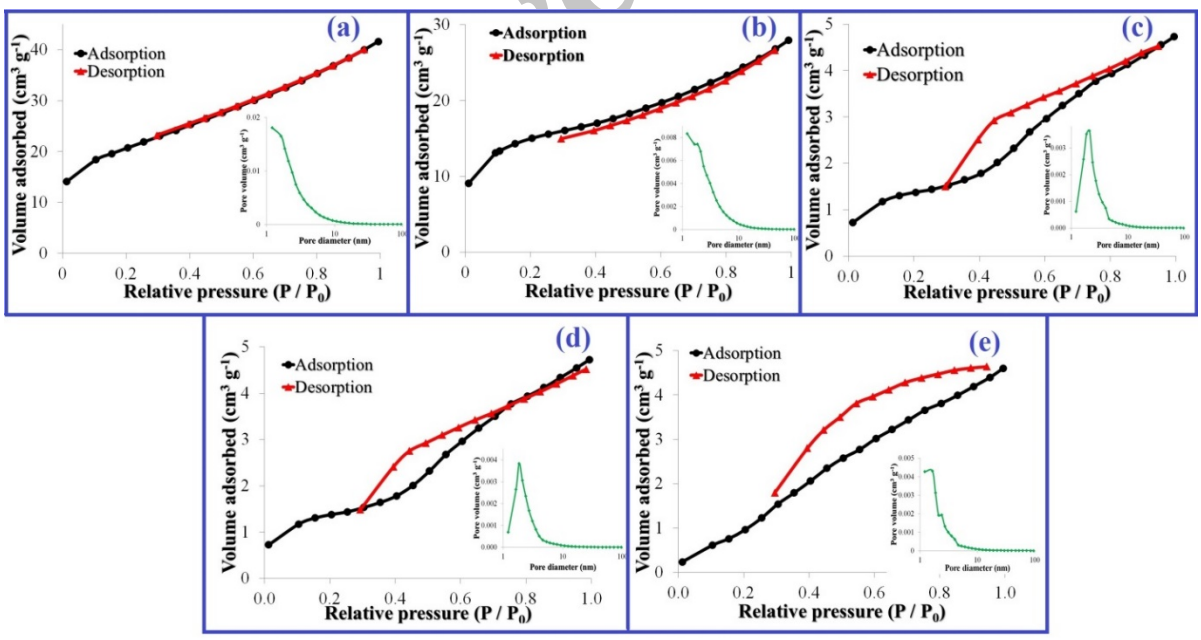

Fig. 5. Nitrogen adsorption and desorption isotherms at liquid nitrogen temperature (77 K) of the (a) LCO-A, (b) LCO-C, (c) LCO-A-1, (d) LCO-C-1 and (e) LCO-C-4, and insets are the corresponding pore size distribution from the adsorption branches of isotherms using BJH model.

N_2 adsorption/desorption for LCO powders synthesized by conventional methods was carried out. Fig. 5 shows the isotherm curves for LCO-A and LCO-C and corresponding samples calcined (LCO-A-1 and LCO-C-1) and also sample calcined in environment oxygen with slow rate (LCO-C-4). Also, BJH pore-size distributions of these samples presented in the insets of Fig. 5, and the corresponding data are presented in Table 3. A strong dependence of the specific surface area on molar ratio can be seen in Table 3.

Table 3. Specific surface areas and pore parameters of LCOs

Sample	S_{BET}[a] (m^2 g^{-1})	V_t[b] (cm^3 g^{-1})	V_{me}[c] (cm^3 g^{-1})	Average pore size[d] (nm)
LCO-A	72.00	0.064	0.052	3.6
LCO-C	52.39	0.043	0.033	3.3
LCO-A-1	4.68	0.007	0.006	6.2
LCO-C-1	4.71	0.006	0.004	5.1
LCO-C-4	7.50	0.007	0.005	3.8

[a] Specific surface area calculated using the BET method.
[b] Total pore volume calculated at P/P_0 =0.99 by the single point method.
[c] Mesopore volume calculated from t-plot method.
[d] Average pore size (D_A), is calculated by $D_A=k * Vt/S_{BET}$, k is 4 using the cylinder model.

The specific surface area of LCO-A to LCO-C decreased sharply from 72 to 52 m^2 g^{-1}. This is due to the higher concentration of nuclei that collide and coalesce resulting in bigger particles with a smaller surface area. After calcination at 800 °C the surface area also decreased sharply.

The observed isotherms for all powders are of the type II, which is most frequently encountered when adsorption occurs on nonporous powders or on powders with pore diameters larger than micro pores [44,45]. The inflection point or knee of the isotherm usually occurs near the completion of the first adsorbed monolayer and with increasing relative pressure, second and higher layers are completed until at saturation the number of adsorbed layers becomes infinite [44]. Furthermore, prominent hysteresis loop is seen at a relative pressure in the range of 0.3−0.9 for calcined powders. BJH pore-size distributions presented in the insets of Fig. 5 show that these samples have micro and mesopores, which confirms the presence of about 1-25 nm pores, as stated above.

On the other hand, by using the shape of the V- t plot it can be determined the type of existing porosity. From Fig. 6, in diagrams LCO-A and LCO-C there are two slope that first slope passes center of the graph and other slope is lower in the previous continue. The two charts show that the powder has micro-pores with the same size. In the early stages of adsorption, absorption values rises rapidly and this is due to the filling of micro cavities. But will not increase the thickness of the adsorbed layer and therefore the elementary slope is

steep. When filling micro pores completed adsorption done only on the surface. At this point slows down the slope. But charts of Fig. 6(c, d and e), which are related to calcinated samples, the slope passes center of the graph are low slope, this slope will be somewhere fast and then slows down gradually. This behavior also can be seen for mesopore adsorbents. These results indicate that the calcinated of LCO powders have major effect on the nature of pores.

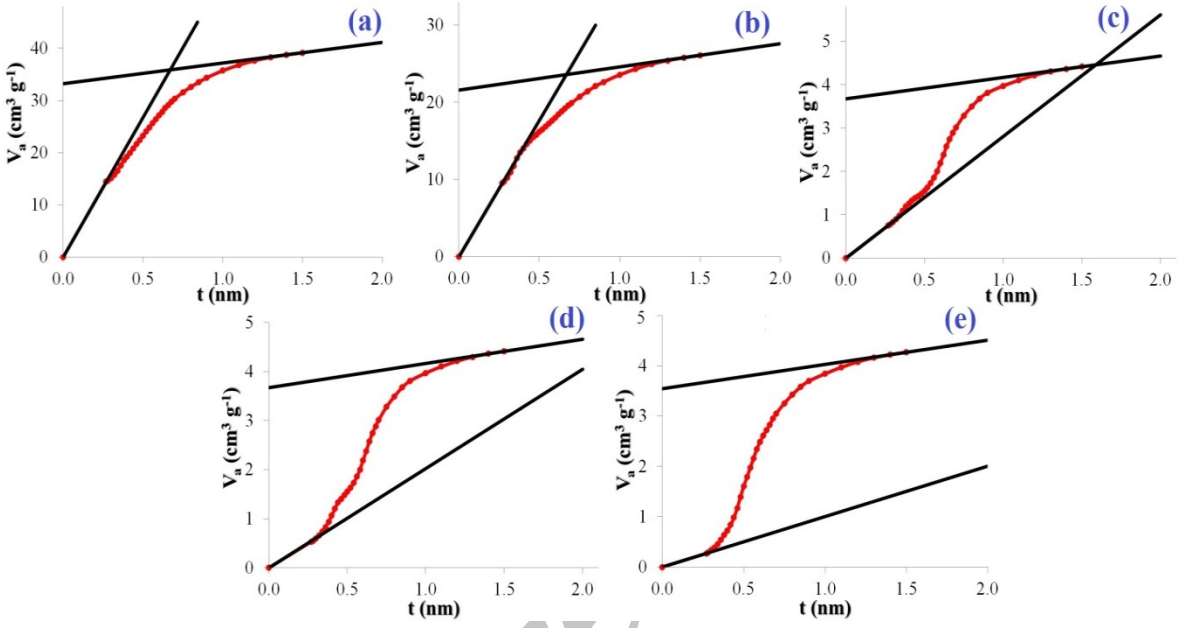

Fig. 6. t-plot of (a) LCO-A, (b) LCO-C, (c) LCO-A-1, (d) LCO-C-1 and (e) LCO-C-4

3.2. Electrochemical measurements

Fig. 7 reveals the charge (Li insertion process)-discharge (Li extraction process) curves of LCOs for the first and second cycles at 0.1 C rates (1 C=280 mA g^{-1}) between 2.5-4.4 V at room temperature and the relevant data are presented in Table 4.

As can be seen, LCOs represent voltage profiles is typical of $LiCoO_2$ Cathodes [46,47]. Charge- discharge results show that the charge capacities of LCO-A-1, LCO-B-1 and LCO-C-1 are 84, 114 and 138 mAh g^{-1}, and the discharge capacities are 68, 96 and 118 mAh g^{-1}, respectively. Comparison of the capacities shows that from LCO-A-1 to LCO-C-1 (with increase of the Co: Li molar ratio) there is an increasing trend. There is also this trend for the capacities second cycle and coloumbic efficiency (CE). Coulombic efficiency is a term used to show ratio discharge capacity to the charge capacity in each cycle. The lower capacity than the theoretical value for the as-synthesized powders can be explained by the large surface area, lower crystallinity, and also by the level of impurities in the powders[48,49].

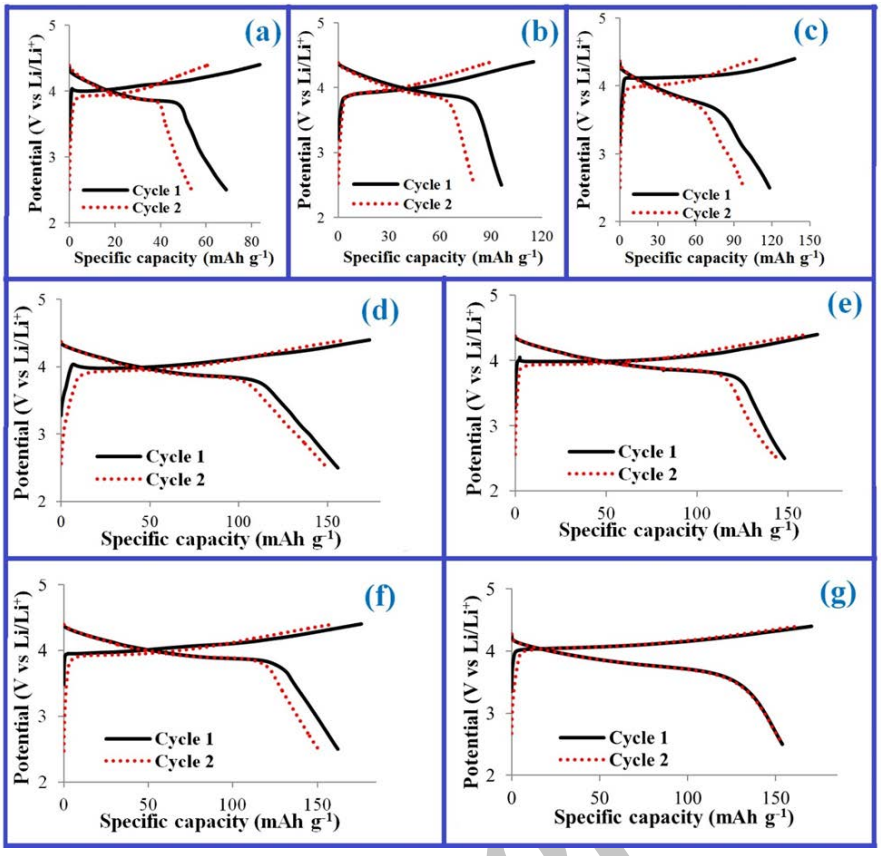

Fig. 7. The first and second galvanostatic charge−discharge profiles of the (a) LCO-A-1, (b) LCO-B-1, (c) LCO-C-1, (d) LCO-C-2, (e) LCO-C-3, (f) LCO-C-4 and (g) LCO-C-5 at 0.1 C (C = 280 mA g^{-1}) within a cutoff voltage window of 2.5−4.4 V

Table 4. The initial charge, reversible and irreversible capacities and coloumbic efficiency obtained from LCO electrodes

Sample	Capacity (mAh g^{-1})				Coloumbic efficiency (%)	
	First cycle		Second cycle			
	Ch[a]	Dis[b]	Ch	Dis	First cycle	Second cycle
LCO-A-1	84	68	62	54	81	87
LCO-B-1	114	96	90	80	84	88
LCO-C-1	138	118	110	98	85	89
LCO-C-2	171	156	161	150	91	93
LCO-C-3	166	148	158	144	89	91
LCO-C-4	176	162	160	150	92	94
LCO-C-5	168	154	162	154	92	95

[a] Charged by a constant current
[b]Discharged by a constant current

Fig. 7(c-g) show charge and discharge curves for LCO samples synthesized under different calcination conditions. The crystallinity of the LCO powders improves at the peak oxygen flow rates. The charge and discharge capacities for the first cycle of three samples LCO-C-3, LCO-C-4 and LCO-C-5 are almost twice other samples. These results are consistent with data obtained from X-ray analysis (percentage LCO crystalline phase was highest in these samples).

Fig. 8 shows cyclic voltammograms of LCO electrodes at 1 mV s^{-1} from 2.5-4.5 V indicative electrochemical activity o [50]. All voltammograms show reversible redox processes at 4.0/3.85 V which refers to the oxidation and reduction of the layered LCOs with Li^+ deinsertion/insertion, respectively. In each voltammogram, a less pronounced peak is also observed at 4.1/4.0 V, which is related to order/disorder phase transitions [51,52].

As for cyclic voltammograms, the separation potential between the anodic and cathodic peaks is an important parameter to value the electrochemical reaction reversibility [53]. As seen, all samples have low reversibility that is related to the rhombohedral structure of LCO, which has Li^+ deficiency and affords the Li^+ insertion with low reversibility. This process could be related to the difference between the volumes of the sites for Li ions insertion in the layered and in the cubic structures, since the tetrahedral sites related to the Li^+ insertion in the cubic structure are smaller than the octahedral sites for the Li^+ insertion in the layered structure. This difference between the volumes of the insertion sites causes a difference between the rates of the Li^+ insertion and, consequently, the low reversibility for the LCO powders [52].

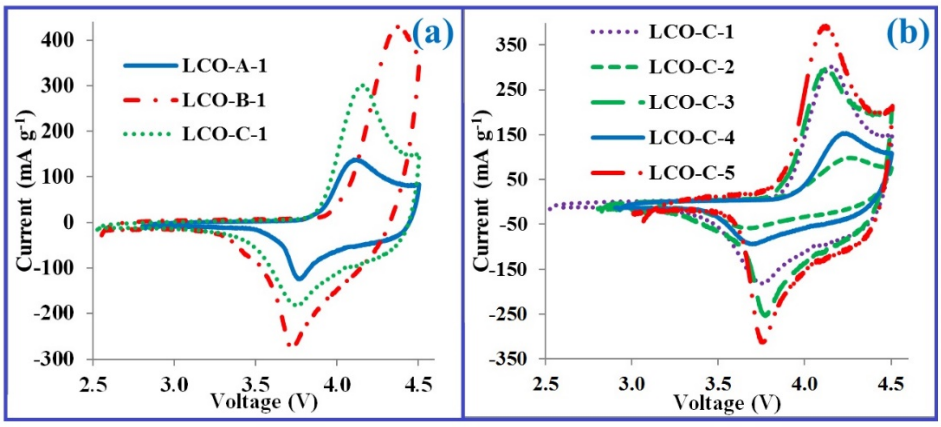

Fig. 8. The Cyclic voltammogram profiles of corresponding to the effect of (a) molar ratios of lithium: cobalt in the precursor solution and (b) calcination environment at a scan rate of 1 mV s^{-1} from about 2.5-4.5 V *vs.* Li/Li^+

Cycling performance of the LCO-C-4 during 50 consecutive charge- discharge cycles is presented in Fig. 9(a). Both specific charge current and discharge current were set to be 1 C.

This electrode exhibited the continuous charge- discharge processes, and capacity retention was 84% after 50 cycles. This indicates that this electrode is stable and appropriate for applications that need to stable cathode over large number of charge-discharge cycles.

In order to investigate the high power performance of the LCO electrodes, each sample was charged at the same rate and discharged at different rates. The obtained capacities were plotted against discharge rate in Fig. 9(b). All of the samples are featured by capacity decay trends with discharge rate. This behavior is inherent to such electrochemical systems having several current dependent capacity fade phenomena which arise from ohmic and charge transfer resistances, and mass transport. Therefore, the lower the resistance, the lower the capacity fade [5]. LCO-A-1, LCO-B-1 and LCO-C-1 have the worst rate capability among LCOs. But, LCO-C-2, LCO-C-3, LCO-C-4 and LCO-C-5 show gentler fade, in comparison.

On the other hand, LCO-C-4 shows the best rate capability. At a high current rate of about 7 C, the reversible capacity still reaches 53 mAh g^{-1}. The reasons for this trend in capacity fading are understood, but certainly is an effect of calcination environment and amount of oxygen during calcination. However, this is not a restrict correlation, and to correlate physical characteristics of the samples to rate capability behavior a comprehensive and dedicated study is required.

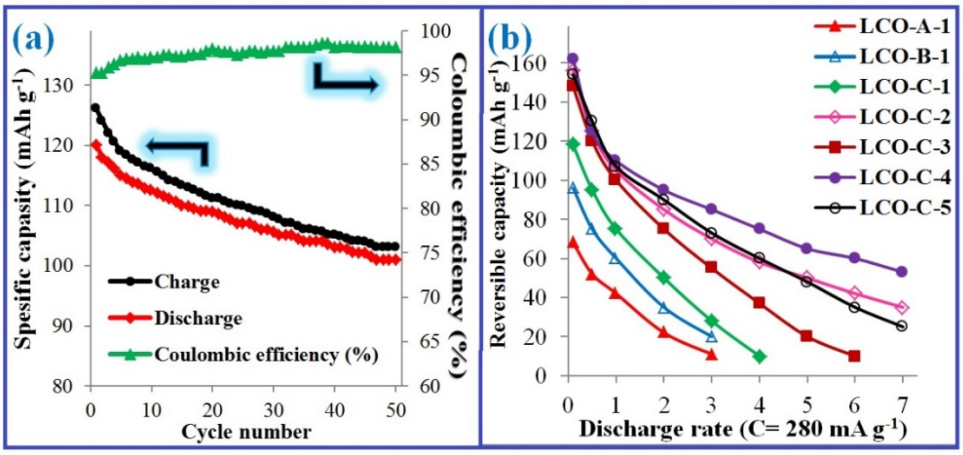

Fig. 9. (a) Cycling performance of LCO-C-4. Charge- discharge cycles were carried out at 1 C between 2.5- 4.4 V for 50 cycles. (b) Reversible capacity versus discharge rate. The samples after charge cycle at 0.1 C to 2.5 V, were discharged with different current rates to 4.4 V

4. CONCLUSION

Spherical, crystalline submicron-sized $LiCoO_2$ powders with surface areas of and single Phase were synthesized using liquid-feed flame spray pyrolysis from the aqueous solutions of nitrates of lithium and cobalt. The effects of changes in molar ratios of lithium to cobalt in the synthesis and different atmospheres for calcination were studied. The residence time of the

particles in the flame at the high temperature region was very short, so only a small portion of layer $LiCoO_2$ decomposed into Co_3O_4. The X-ray diffraction patterns of samples after calcination have a pure crystalline LCO rhombohedral phase. Physical and functional characterization of electrodes made by these samples was investigated. The capacity of the as-synthesized powders can be explained by the surface area, crystallinity, and also by the level of impurities in the powders. The results showed that the samples obtained in oxygen environment with low flow, a lithium cobalt oxide phase pure crystalline rhombohedral and it also has the best performance electrode electrochemical cyclic voltammetry analysis of all samples synthesized.

Acknowledgements

The authors would like to thank the University of Isfahan for providing facilities and financial support.

REFERENCES

[1] M. Winter, and R. J. Brodd, Chem. Rev. 104 (2004) 4245.
[2] D. Larcher, and J. Tarascon, Nature Chem. 7 (2015) 19.
[3] Y. G. Guo, J. S. Hu, and L. J. Wan, Adv. Mater. 20 (2008) 2878.
[4] A. S. Arico, P. Bruce, B. Scrosati, J. M. Tarascon, and W. Van Schalkwijk, Nature Mater. 4 (2005) 366.
[5] S. M. Jafari, M. Khosravi, and M. Mollazadeh, Electrochim. Acta 203 (2016) 9.
[6] K. Mizushima, P. Jones, P. Wiseman, and J. Goodenough, Mater. Res. Bulletin 15 (1980) 783.
[7] H. Chen, X. Qiu, W. Zhu, and P. Hagenmuller, Electrochem. Commun. 4 (2002) 488.
[8] P. Poizot, S. Laruelle, S. Grugeon, L. Dupont, and J. Tarascon, Nature 407 (2000) 496.
[9] W. Y. Teoh, R. Amal, and L. Mädler, Nanoscale 2 (2010) 1324.
[10] Z. Ma, X. Yuan, L. Li, Z. F. Ma, D. P. Wilkinson, and L. Zhang, Energy Environ. Sci. 8 (2015) 2144.
[11] Y. Gan, L. Zhang, Y. Wen, F. Wang, and H. Su, Particuology 6 (2008) 81.
[12] P. He, H. Yu, and H. Zhou, J. Mater. Chem. 22 (2012) 3680.
[13] Y. Gu, D. Chen, and X. Jiao, J. Phys. Chem. B109 (2005) 17901.
[14] C. D. Snyders, E. E. Ferg, J. Schuelein, and H. Loewe, South African J. Chem. 69 (2016) 88.
[15] K. K. Bokinala, M. Pollet, A. Artemenko, M. Miclau, and I. Grozescu, J Solid State Chem. 198 (2013) 45.
[16] Y. Tao, B. Zhu, and Z. Chen, J. Alloys Comp. 430 (2007) 222.
[17] D. S. Jung, S. B. Park, and Y. C. Kang, Korean J. Chem. Eng. 27 (2010) 1621.

[18] J. H. Bang, K. Han, S. E. Skrabalak, H. Kim, and K. S. Suslick, J. Phys. Chem. C 111 (2007) 10959.
[19] R. Strobel and S. E. Pratsinis, Platinum Metals Rev. 53 (2009) 11.
[20] R. Strobel, A. Baiker, and S. E. Pratsinis, Adv. Powder Technol. 17 (2006) 457.
[21] T. Xia, M. Kovochich, M. Liong, L. Mädler, B. Gilbert, and H. Shi, ACS nano 2 (2008) 2121.
[22] L. Mädler, T. Sahm, A. Gurlo, J.-D. Grunwaldt, N. Barsan, and U. Weimar, J. Nanoparticle Res. 8 (2006) 783.
[23] T. Patey, R. Büchel, M. Nakayama, and P. Novak, Phys. Chem. Chem. Phys. 11 (2009) 3756.
[24] S. H. Ng, T. J. Patey, R. Büchel, F. Krumeich, J. Z. Wang, and H. K. Liu, Phys. Chem. Chem. Phys. 11 (2009) 3748.
[25] Y. Li, Y. Hu, J. Huo, H. Jiang, C. Li, and G. Huang, Indust. Eng. Chem. Res. 51 (2012) 11157.
[26] P. Pawinrat, O. Mekasuwandumrong, and J. Panpranot, Catalysis Commun. 10 (2009) 1380.
[27] J. A. Azurdia, J. Marchal, P. Shea, H. Sun, X. Q. Pan, and R. M. Laine, Chem. Mater. 18 (2006) 731.
[28] T. Sahm, L. Mädler, A. Gurlo, N. Barsan, S. Pratsinis, and U. Weimar, Sens. Actuators B 98 (2004) 148.
[29] R. M. Laine, J. Marchal, H. Sun, and X. Q. Pan, Adv. Mater. 17 (2005) 830.
[30] R. M. Laine, C. R. Bickmore, D. R. Treadwell, and K. F. Waldner, Ultrafine metal oxide powders by flame spray pyrolysis, ed: Google Patents, (1999).
[31] J. A. Azurdia, J. Marchal, P. Shea, H. Sun, X. Q. Pan, and R. M. Laine, Chem. Mater. 18 (2006) 731.
[32] R. Baranwal, M. P. Villar, R. Garcia, and R. M. Laine, J. Am. Ceramic Soc. 84 (2001) 951.
[33] A. Purwanto, W.-N. Wang, and K. Okuyama, Flame Spray Pyrolysis, in Handbook of Atomization and Sprays, ed: Springer (2011) pp. 869-879.
[34] N. Wagner, A. M. Svensson, and F. Vullum-Bruer, Translational Mater. Res. 3 (2016) 025001.
[35] R. Laine, J. Marchal, H. Sun, and X. Pan, Nature Mater. 5 (2006) 710.
[36] A. Singh, and D. Lal, J. Appl. Poly. Sci. 100 (2006) 2323.
[37] R. Gummow, D. Liles, and M. Thackeray, Mater. Res. Bulletin 28 (1993) 235.
[38] M. Sathiya, A. S. Prakash, K. Ramesha, and A. K. Shukla, Materials 2 (2009) 857.
[39] R. Alcantara, P. Lavela, J. Tirado, E. Zhecheva, and R. Stoyanova, J. Solid State Electrochem. 3 (1999) 121.
[40] O. Carp, C. L. Huisman, and A. Reller, Progress Solid State Chem. 32 (2004) 33.

[41] M. Inagaki, R. Nonaka, B. Tryba, and A. W. Morawski, Chemosphere 64 (2006) 437.
[42] C. Julien, M. Camacho-Lopez, T. Mohan, S. Chitra, P. Kalyani, and S. Gopukumar, Solid State Ionics 135 (2000) 241.
[43] L. Li, W. H. Meyer, G. Wegner, and M. Wohlfahrt-Mehrens, Adv. Mater. 17 (2005) 984.
[44] S. Lowell and J. E. Shields, Powder surface area and porosity, Springer Science & Business Media vol. 2 (2013).
[45] K. S. Sing, Pure Appl. Chem. 57 (1985) 603.
[46] A. Kannan, L. Rabenberg, and A. Manthiram, Electrochem. solid-state Lett. 6 (2003) A16.
[47] X. Li, F. Cheng, B. Guo, and J. Chen, J. Phys. Chem. B 109 (2005) 14017.
[48] Y. K. Sun, I. H. Oh, and S. A. Hong, J. Mater. Sci. 31 (1996) 3617.
[49] K. Kanamura, A. Goto, R. Y. Ho, T. Umegaki, K. Toyoshima, and K. i. Okada, Electrochem. Solid-State Lett. 3 (2000) 256.
[50] K. Shaju, G. S. Rao, and B. Chowdari, Electrochim. Acta 48 (2002) 145.
[51] M. Antaya, K. Cearns, J. Preston, J. Reimers, and J. Dahn, J. Appl. Phys. 76 (1994) 2799.
[52] E. Santiago, A. Andrade, C. Paiva-Santos, and L. Bulhoes, Solid State Ionics 158 (2003) 91.
[53] J. Ni, H. Zhou, J. Chen, and X. Zhang, Mater. Lett. 59 (2005) 2361.